THE JOURNAL OF
PHYSICAL CHEMISTRY C

Article

pubs.acs.org/JPCC

Composition–Structure–Activity Correlation of Platinum–Ruthenium Nanoalloy Catalysts for Ethanol Oxidation Reaction

Yinguang Zhao,[†] Yazan Maswadeh,[‡] Shiyao Shan,[†] Hannah Cronk,[†] Zakiya Skeete,[†] Binay Prasai,[‡] Jin Luo,[†] Valeri Petkov,*[,‡] and Chuan-Jian Zhong*[,†]

[†]Department of Chemistry, State University of New York at Binghamton, Binghamton, New York 13902, United States

[‡]Department of Physics, Central Michigan University, Mt. Pleasant, Michigan 48859, United States

Supporting Information

ABSTRACT: Understanding the evolution of the composition and atomic structure of nanoalloy catalysts in the ethanol oxidation reaction (EOR) is essential for the design of active and robust catalysts for direct ethanol fuel cells. This article describes a study of carbon-supported platinum–ruthenium electrocatalysts (PtRu/C) with different bimetallic compositions and their activities in the EOR, an important anode reaction in direct ethanol fuel cells (DEFCs). The study focused on establishing the relationship between the catalyst's composition, atomic structure, and catalytic activity for the EOR. Ex situ and in situ synchrotron high-energy X-ray diffraction (HE-XRD) experiments coupled with atomic pair distribution function (PDF) analysis and in situ energy-dispersive X-ray (EDX) analysis were employed to probe the composition and structural evolution of the catalysts during the in situ EOR inside a membrane electrode assembly (MEA) in the fuel cell. The results revealed an intriguing composition–structure–activity relationship for the PtRu electrocatalysts under EOR experimental conditions. In particular, the alloy with a Pt/Ru ratio of ~50:50 was found to exhibit a maximum EOR activity as a function of the bimetallic composition. This composition–activity relationship coincides with the relationship between the Pt interatomic distances and coordination numbers and the bimetallic composition. Notably, the catalytic activities of the PtRu electrocatalysts showed a significant improvement during the EOR, which can be related to atomic-level structural changes in the nanoalloys occurring during the EOR, as indicated by in situ HE-XRD/PDF/EDX data. The findings shed some new light on the mechanism of the ethanol oxidation reaction over bimetallic alloy nanocatalysts, which is important for the rational design and synthesis of active nanoalloy catalysts for DEFCs.

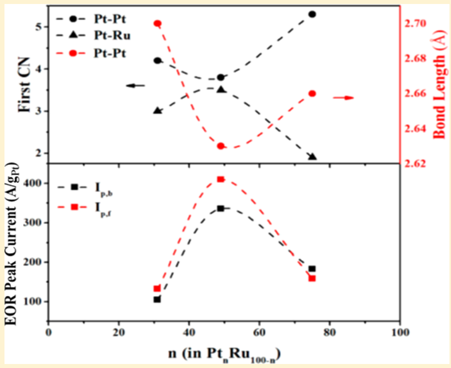

1. INTRODUCTION

The development of direct ethanol fuel cells (DEFCs) as a power source has drawn a surge of interest in recent years because of their high energy density (8.0 kW h kg^{-1}), low toxicity, and ease of storage and transportation. In addition, ethanol is biorenewable, and it can be produced in large amounts through the fermentation of sugar cane, corn, or wheat. One of the key issues in the development of ethanol-based fuel cells is the need for highly effective, robust, and low-cost catalysts.[1,2] However, the slow kinetics of the catalytic ethanol oxidation reaction is still a barrier to the development and commercialization of DEFCs. Platinum is a highly active catalyst for most fuel-cell reactions, including the oxygen reduction reaction and small-molecule oxidation reactions. However, pure platinum is not effective for the electro-oxidation of ethanol because it can be easily poisoned by strongly adsorbed intermediates, such as CO.[3−11] Several studies of alloys of Pt with different transition metals, such as PtRu, PtSn, PtPd, and PtRh, have been performed in efforts to increase the catalytic activity and reduce the cost.[12−15] Ternary catalysts such as Pt/Rh/SnO_2 have been shown to be able to break the C–C bond of ethanol and produce CO_2 in an acidic electrolyte.[16] Binary catalysts such as PdCu have recently been shown to exhibit catalytic activity for oxidizing ethanol to CO_2 in an alkaline electrolyte.[17]

Among different binary catalysts, there have been extensive studies of PtRu for the methanol oxidation reaction (MOR). However, limited studies have been reported for the ethanol oxidation reaction (EOR) over PtRu. In comparison with Pt, Ru has a lower oxidation potential for H_2O.[18] In general, a bifunctional mechanism has been proposed for PtRu, whereby ethanol adsorbed on Pt forms a strong bond and its oxidized species can be removed by oxygen-containing species formed on Ru. In a recent study of the EOR, PtRu alloy catalysts with different atomic ratios prepared by the electrodeposition method displayed an increased activity with Ru contents of up to 40%.[19] Ru is believed to facilitate the oxidation of intermediates and not to increase the selectivity for complete oxidation toward CO_2.[20] The activity depends strongly on the preparation method, as shown by differences in EOR activity

Received: April 26, 2017
Revised: July 19, 2017

DOI: 10.1021/acs.jpcc.7b03901

over PtRu prepared by the coreduction of mixed ions[21] and with different degrees of alloying.[22] High-surface-area metal oxides, such as TiO_2 and SnO_2, have been investigated as additives in PtRu/C catalysts to enhance the electro-oxidation of ethanol in acidic solution. The PtRu-based composite catalyst containing a SnO_2 promoter exhibited a lower onset potential and a higher current density for ethanol oxidation than both the additive-free catalyst and the catalyst containing TiO_2 promoter.[23] The highly active Fe−N−C catalyst has been investigated to gain insight into its extraordinary tolerance to the presence of alcohols.[24]

Despite these prior studies, the mechanism of the EOR over PtRu catalysts remains unclear, and some of the previous results are not fully understood. For example, PtRu catalysts with 50−60% Pt were shown to exhibit the highest EOR activity in some studies,[19,25] whereas a Pt content of ~30% was found to be the most catalytically active composition in another study.[21] In view of the fact that catalysts prepared or treated by different methods have shown different catalytic activities,[22] there is a need to understand how different synthesis methods and treatment processes correlate with the atomic structure of the alloy nanoparticles. In our recent work, the three-dimensional atomic structures of Pt_nRu_{100-n} (n = 31, 49, 75) catalysts were characterized by total scattering experiments involving ex situ high-energy synchrotron X-ray diffraction (HE-XRD) in conjunction with the analysis of atomic pair distribution functions (PDFs) and reverse Monte Carlo (RMC) modeling,[25] which provided new structural information on the nanoalloy catalysts. We report herein new findings from an investigation of the correlation of the structure of PtRu nanocatalysts with their EOR activity, including an in situ study of the catalysts in a membrane electrode assembly (MEA) of an ethanol vapor fuel cell under half-cell measurement conditions. As illustrated in Scheme 1, the three-dimensional structural parameters from the HE-XRD/PDF/RMC analyses[25] can be used to understand the correlation between the bimetallic composition and the catalytic activity.

Scheme 1. Illustration of Models of PtRu Nanoalloys with Different Compositions Derived from the HE-XRD/PDF/RMC Study[25] Used for Understanding of the Correlation between Composition and Activity

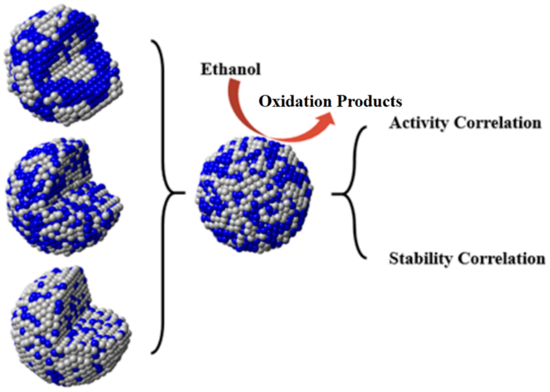

2. EXPERIMENTAL SECTION

2.1. Chemicals. Platinum(II) acetylacetonate [$Pt(acac)_2$, 97%], ruthenium(III) acetylacetonate [$Ru(acac)_3$, 97%], octyl ether (99%), oleylamine (70%), 1,2-hexadecanediol (90%), and oleic acid (>99%) were purchased from Aldrich. Other chemicals such as ethanol, hexane, and potassium chloride were purchased from Fisher Scientific. Vulcan carbon XC-72 was obtained from Cabot. All gases were obtained from Airgas. All chemicals were used as received. Water was purified with a Millipore Milli-Q water system.

2.2. Synthesis and Preparation. Pt_nRu_{100-n} nanoparticles (NPs) (n = 31, 49, and 75) were synthesized according to a protocol described previously.[25] In brief, platinum(II) acetylacetonate and ruthenium(III) acetylacetonate were mixed in the desired molar ratio in octyl ether solution under a N_2 atmosphere. Oleic acid and oleylamine were added to the solution as NP capping agents, and 1,2-hexadecanediol was added as a reducing agent. The solution was purged with N_2, heated to 220 °C, and kept at that temperature for 30 min. After the solution had cooled to room temperature, the resulting PtRu NPs were precipitated by adding ethanol and separated from the solution by centrifugation. The precipitated NPs were redispersed in hexane and mixed with fine carbon powder (XC-72), and the resulting mixture was subjected to sonication and overnight stirring. The resulting carbon-supported PtRu NPs, hereafter referred to as the as-synthesized NPs, were collected and dried under a N_2 atmosphere. The carbon-supported PtRu NPs were activated for catalytic applications. The activation involved a two-step thermal treatment under a controlled gas atmosphere.[25] In particular, the PtRu NPs were first heated to 260 °C under a N_2 atmosphere to remove the organic molecules from the NP surface. Next, the NPs were further heated to 400 °C under a 15 vol % H_2 atmosphere and held at that temperature for 2 h. The postsynthesis-treated NPs are hereafter referred to as the fresh catalysts or Pt_nRu_{100-n}/C (n = 31, 49, and 75) catalysts.

2.3. Characterization of Catalysts. *2.3.1. Thermogravimetric Analysis (TGA).* The loading of PtRu NPs on the carbon support was determined by thermogravimetric analysis (TGA) performed on a Perkin-Elmer Pyris 1-TGA instrument and was found to be within the range of 15−30 wt %. The nanoparticles were mixed with carbon (20% metal loading) before thermal treatment. The measured loadings were 20% for $Pt_{31}Ru_{69}/C$, 19% for $Pt_{49}Ru_{51}/C$, and 29% for $Pt_{75}Ru_{25}/C$. For $Pt_{75}Ru_{25}/C$, the degree of burning of the carbon support was found to be somewhat higher than that for the other PtRu catalysts.

2.3.2. Inductively Coupled Plasma-Atomic Emission Spectroscopy (ICP-AES). ICP-AES was used to analyze the chemical compositions of the as-synthesized and fresh PtRu alloy NPs. The analysis was performed on a Perkin-Elmer 2000 DV ICP optical emission spectrometer using a cross-flow nebulizer with the following parameters: plasma, 18.0 L of Ar(g)/min; auxiliary, 0.3 L of Ar(g)/min; nebulizer, 0.73 L of Ar(g)/min; power, 1500 W; peristaltic pump rate, 1.40 mL/min. Samples were dissolved in aqua regia and then diluted to concentrations in the range of 1−50 ppm. Calibration curves were made from dissolved standards in the same acid matrix as the unknowns. The standards and the unknowns were analyzed 10 times each, resulting in <3% error in the reported chemical compositions. Within the error limits, no appreciable differences between the chemical compositions of the as-synthesized and corresponding fresh PtRu NPs were observed. Note that similar thermochemical activation of noble-metal-based NPs for catalytic applications was also shown not to induce significant changes in NP's overall chemical composition, size, or shape.[26]

2.3.3. Transmission Electron Microscopy (TEM). TEM and high-resolution TEM (HR-TEM) were employed to determine the sizes and morphologies of the as-synthesized and fresh

PtRu NPs. For the measurements, batches of NPs were diluted in hexane and drop cast onto carbon-coated copper grids; the solvent was then allowed to evaporate in air at room temperature. The measurements were performed on a JEM-2200FS microscope operated at 200 kV. The microscope was fitted with an ultrahigh-resolution (UHR) pole piece with a point resolution of 0.19 nm.

2.3.4. High-Angle Annular Dark-Field (HAADF) Scanning TEM (STEM). The chemical patterns of fresh PtRu NPs were determined by HAADF-STEM. Experiments were performed on a JEOL JEM 2100F instrument equipped with a CEOS hexapole probe. The instrument was operated at 200 keV in STEM mode. The lens settings combined with the corrector tuning gave a spatial resolution of ~90 pm.

2.3.5. Catalytic Activity Measurements. The catalytic activities of fresh Pt_nRu_{100-n}/C (n = 31, 49, and 75) catalysts for the electrocatalytic oxidation of ethanol were measured following a typical procedure reported previously.[17] In brief, glassy carbon (GC) disks (geometric area = 0.07 cm^2) were polished with 0.005-μm Al_2O_3 powders. A typical suspension of the carbon-supported catalysts was prepared by adding 5 mg of catalyst (fresh PtRu/C) to 5 mL of 0.25% Nafion solution and ultrasonicating the mixture for 10 min until it became a uniform dark ink. Then, 5 μL of the suspension was quantitatively transferred to the surface of the polished 0.07 cm^2 GC disk.[27] The disk, as coated with a thin film of the ink, was dried overnight at room temperature, inserted into an electrochemical cell, and used as the cell's working electrode. The cell included two additional electrodes: a reference electrode [Ag/AgCl, saturated KCl, or saturated calomel electrode (SCE)] and a counter electrode (Pt). Cyclic voltammetry (CV) was performed using a microcomputer-controlled electrochemical analyzer (CHI600a, CH Instruments) at room temperature. The electrolyte (0.1 M $HClO_4$) was deaerated with high-purity N_2 before cyclic voltammetry (CV) measurements were conducted. Current generated by the cell was measured as the potential of the working electrode was varied. Ethanol was added to the electrolyte for the study of oxidation. For the analysis of the CV curves, $I_{p,f}$ and $E_{p,f}$ represent the ethanol oxidation peak current and potential, respectively, in the negative-to-positive sweep direction, and $I_{p,b}$ and $E_{p,b}$ represent the same quantities in the reverse sweep direction. $E_{p,f}'$, $E_{p,b}'$, $I_{p,f}'$, and $I_{p,b}'$ represent the same peak potentials and currents in the CV curves of the catalysts after they had been subjected to potential cycling.

2.3.6. Ex Situ/In Situ Synchrotron High-Energy XRD (HE-XRD). Ex situ HE-XRD measurements of the carbon-supported as-synthesized and fresh Pt_nRu_{100-n} (n = 31, 49, and 75) catalysts were carried out at Sector 11 of the Advanced Photon Source, Argonne National Laboratory. X-rays with an energy of 115 keV (λ = 0.1080 Å) were used. Diffraction data were collected on a large-area detector up to wave vectors of 25 $Å^{-1}$, allowing for the resolution of the structural features of the PtRu NPs in fine detail. The experimental setup was calibrated with high-purity powder Si standard. During the measurements, samples were sealed in thin-walled glass capillaries.

In situ HE-XRD measurements of fresh $Pt_{49}Ru_{51}/C$ catalyst were carried out at Sector 1 of the Advanced Photon Source, Argonne National Laboratory. X-rays with an energy of 100.2 keV (λ = 0.1236 Å) were used. Measurements were carried out on MEAs in a custom-built fuel cell that was optimized for HE-XRD.[28] MEAs containing $Pt_{49}Ru_{51}/C$ (19% metal loading, 0.6 mg of Pt/cm^2) as the anode catalyst and Pt/C (20% Pt/C, Etek, 0.08 mg of Pt/cm^2) as the cathode catalyst on carbon papers were prepared. Whereas the carbon-paper electrode was 2.5 × 2.5 cm^2, the effective geometric area of catalyst on the carbon paper was 3.10 cm^2. The MEAs were prepared by hot pressing the sandwich-structured Nafion membrane (Nafion 212) and catalyst-coated electrodes at 120 °C. The MEAs were tested at 75 °C with 100% humidified 3% H_2 (balanced by N_2) fed to the cathode at a flow rate of 50 mL/min, which functioned as a dynamic hydrogen electrode (DHE) for the in situ half-cell reaction measurements. Ethanol vapor was carried by N_2 at a flow rate of 50 mL/min and introduced onto the anode, where the EOR half-cell reaction occurred. In situ HE-XRD and energy-dispersive X-ray (EDX) data were collected in intervals of 1 min as the cell's anode was cycled in the potential range of 0−1.2 V at a scan rate of 100 mV/s for ~90 min, amounting to about 200 cycles. The HE-XRD patterns were reduced to so-called structure atomic pair distribution functions (PDFs), which have proven to be highly advantageous in structural studies of metallic alloy catalysts.[25,28−30]

3. RESULTS AND DISCUSSION

3.1. Composition and Structure of PtRu Nanoparticles. The relationship between the Pt composition in PtRu NPs and the synthetic feeding composition is shown in Figure 1. Data for the composition of PtRu NPs shows a slope of 0.88, which is slightly less than 1, indicating that the chemical composition of the binary alloy PtRu NPs can be controlled well by controlling the feed ratio of the metal precursors during the synthesis. This finding indicates that Pt is slightly more favored than Ru in the formation of the bimetallic nanoparticles.

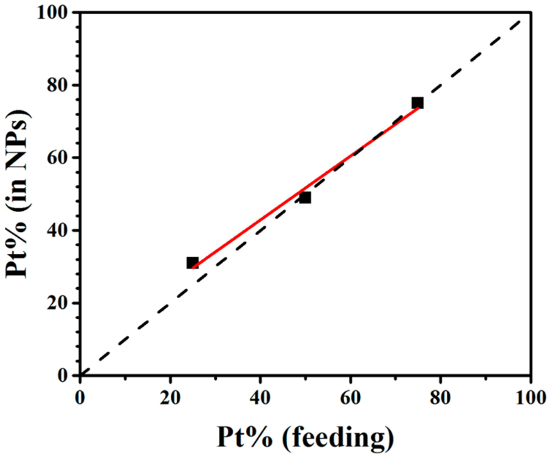

Figure 1. Plot of Pt composition in PtRu NPs (from ICP-AES analysis) vs synthetic feeding composition. The dashed line represents a 1:1 relationship. The solid line represents the linear fitting to the actual nanoparticle data (slope = 0.88, R^2 = 0.978).

Figure 2 shows a representative set of TEM, HR-TEM, and HAADF-STEM images of Pt_nRu_{100-n}/C [n = 31 (Figure 2A), 49 (Figure 2B), and 75 (Figure 2C)] catalysts after thermal treatment. The PtRu NPs feature an average size of 4.6 (±0.7) nm and display good crystallinity. $Pt_{49}Ru_{51}/C$ and $Pt_{75}Ru_{25}/C$ exhibit quite uniform contrast, indicating single-phase compositions, whereas $Pt_{31}Ru_{69}/C$ shows some bright and dark contrast patterns, indicating phase-segregated [Pt-rich (bright) and Ru-rich (dark)] domains. $Pt_{75}Ru_{25}/C$ displays a lattice fringe of 0.222 nm, characteristic of the {111} plane of the fcc

DOI: 10.1021/acs.jpcc.7b03901
J. Phys. Chem. C XXXX, XXX, XXX−XXX

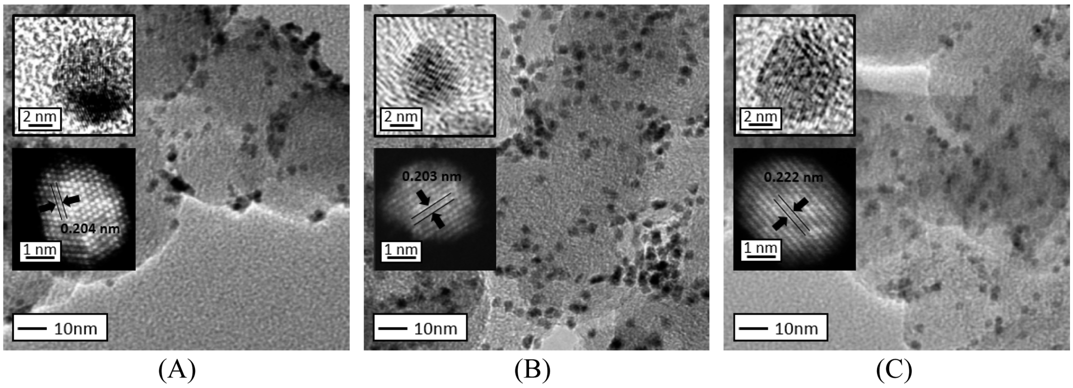

(A) (B) (C)

Figure 2. TEM images of (A) $Pt_{31}Ru_{69}/C$, (B) $Pt_{49}Ru_{51}/C$, and (C) $Pt_{75}Ru_{25}/C$ after thermal treatment. Insets: (top) HR-TEM images and (bottom) HAADF-STEM images of the respective catalysts.

structure.[31−34] $Pt_{31}Ru_{69}/C$ and $Pt_{49}Ru_{51}/C$ exhibit lattice fringes of 0.204 and 0.203 nm, respectively, corresponding to the {200} plane of the fcc structure.[35]

The lattice parameters of the Pt_nRu_{100-n}/C (n = 31, 49, and 75) NPs, as determined from HE-XRD/PDF data,[25] were analyzed (Figure 3). The results indicate that $Pt_{75}Ru_{25}/C$ is fcc-type ordered, $Pt_{49}Ru_{51}/C$ is largely fcc-type ordered, and $Pt_{31}Ru_{69}/C$ is segregated into fcc and hcp domains. The addition of Ru has a contraction effect. Apparently, the lattice parameters do show some agreement with the lattice parameters of Pt and Ru as a function of composition (dashed lines). Here, we investigated $Pt_{49}Ru_{51}/C$ further by applying atomic PDF analysis. The results showed that $Pt_{49}Ru_{51}/C$ is a stack of close-packed atomic layers. About 80% of the layers in the stack follow an fcc-type packing sequence. The remaining 20% can be viewed as stacking faults introducing an hcp character of the atomic structure. Note that the presence of stacking faults does not imply phase segregation. It merely reflects the lack of perfect three-dimensional periodicity in the atomic ordering in the NPs.

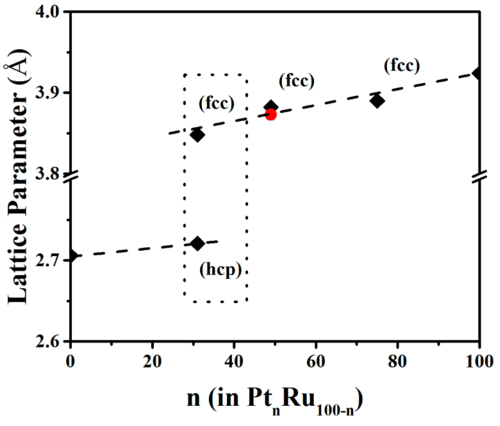

Figure 3. Lattice parameters (calculated from PDFs) vs composition for Pt_nRu_{100-n} (n = 31, 49, and 75). Dashed lines are the fitting relationships between metal and PtRu NPs. The dashed box for $Pt_{31}Ru_{69}$ indicates the co-existence of hcp and fcc phases. Black squares are data extracted from a recent report.[25] The red circle indicates data extracted from the study reported herein.

Key findings of the prior and present structure studies are summarized in Figure 4 in terms of bond lengths (Figure 4A) and first coordination numbers (CNs) of atoms on the surface of fresh Pt_nRu_{100-n}/C (n = 31, 49, and 75) catalysts (Figure 4B).[25] A maximum for the Ru−Ru bond length and a minimum for the Pt−Pt bond length were observed for PtRu NPs with a Pt/Ru ratio of 49:51. Interestingly, a maximum of the Pt−Ru first CN and a minimum of the Pt−Pt first CN were also observed for atoms on the surface of $Pt_{49}Ru_{51}/C$. These maximum and minimum features from PDFs can be linked to the catalytic activity for the EOR, providing important information for assessing the structure−activity relationship, especially the changes in composition or atomic structure

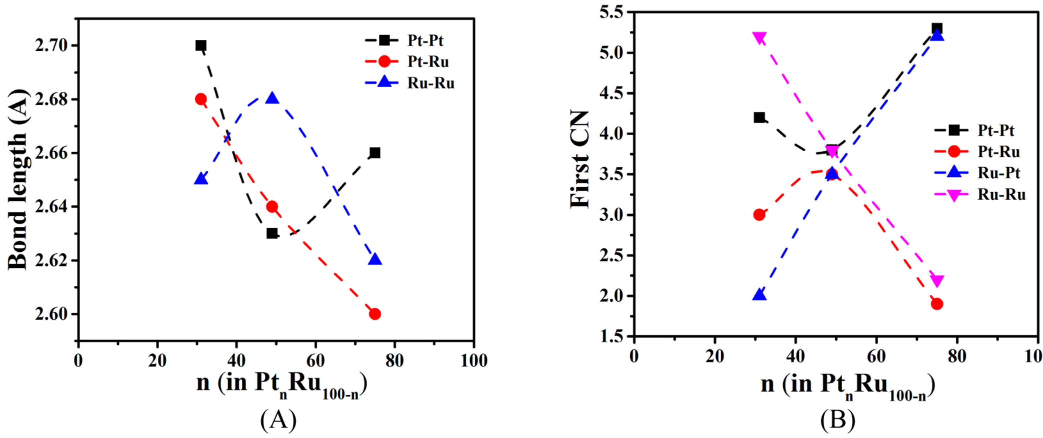

Figure 4. Plots of (A) bond length and (B) first CN for atoms on the surface of fresh Pt_nRu_{100-n}/C (n = 31, 49, and 75) NPs as a function of the bimetallic composition.

DOI: 10.1021/acs.jpcc.7b03901
J. Phys. Chem. C XXXX, XXX, XXX−XXX

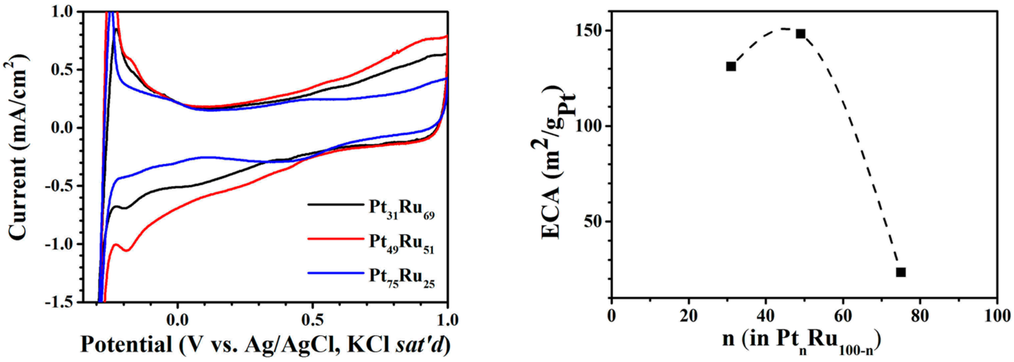

(A) (B)

Figure 5. (A) CV curves and (B) ECA plot for Pt_nRu_{100-n}/C (n = 31, 49, and 75) catalysts. Electrode, glassy carbon (0.07 cm^2) inked with 5 μg of catalyst; electrolyte, 0.1 M $HClO_4$ saturated with N_2; scan rate, 50 mV/s.

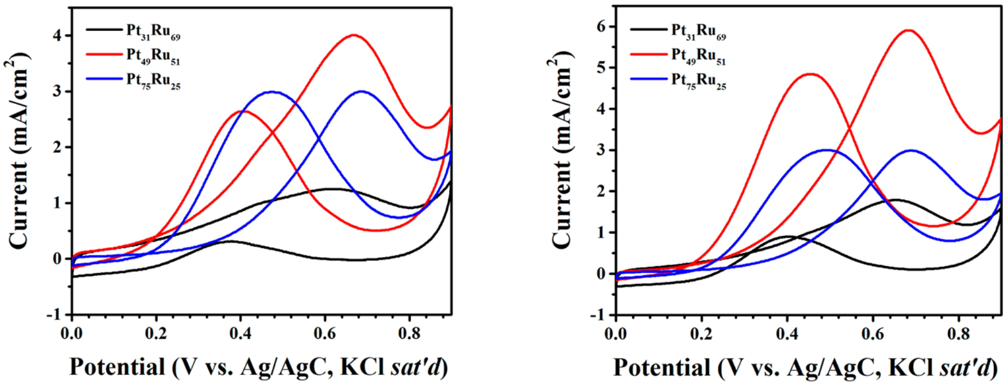

(A) (B)

Figure 6. CV curves for (A) fresh Pt_nRu_{100-n}/C (n = 31, 49, and 75) catalysts and (B) the same catalysts after 30 potential cycles. Electrode, glassy carbon (0.07 cm^2) inked with 5 μg of catalyst; electrolyte, 0.1 M $HClO_4$ with 0.5 M ethanol saturated with N_2; scan rate, 50 mV/s.

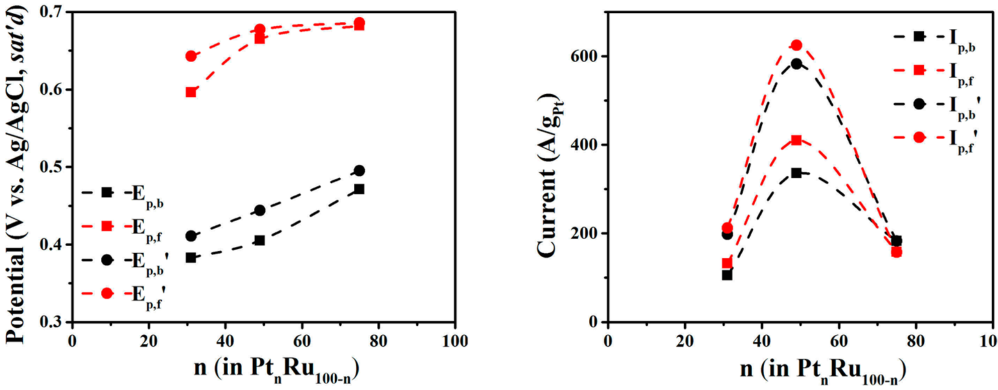

(A) (B)

Figure 7. (A) EOR peak potentials for the fresh catalysts ($E_{p,b}$ and $E_{p,f}$) and the same catalysts after 30 potential cycles ($E_{p,b}'$ and $E_{p,f}'$). (B) EOR peak currents for the fresh catalysts ($I_{p,b}$ and $I_{p,f}$) and the same catalysts after 30 potential cycles ($I_{p,b}'$ and $I_{p,f}'$). Electrolyte, 0.1 M $HClO_4$ with 0.5 M ethanol saturated with N_2; scan rate, 50 mV/s. Data extracted from Figure 6.

occurring during electrochemical processes, as discussed in the next subsections.

3.2. Electrocatalytic Properties in Acidic Electrolyte.

The as-prepared Pt_nRu_{100-n}/C (n = 31, 49, and 75) catalysts were examined using the CV technique to determine their electrochemically active areas (ECAs). The electrochemical measurements were performed after 30 potential cycles between −0.3 and 1.0 V (vs Ag/AgCl, saturated KCl) in N_2-saturated 0.1 M $HClO_4$ solution at 50 mV/s, which activated the catalysts. Figure 5A shows a typical set of initial CV curves after activation for catalysts with different compositions ($Pt_{31}Ru_{69}$/C, $Pt_{49}Ru_{51}$/C, and $Pt_{75}Ru_{25}$/C). The voltammetric characteristics in the hydrogen adsorption/desorption range (from −0.23 to 0.20 V vs Ag/AgCl, saturated KCl) showed significant differences for different compositions. $Pt_{49}Ru_{51}$/C exhibited the largest hydrogen adsorption peak, indicative of the largest ECA value (see Figure 5B), whereas $Pt_{75}Ru_{25}$/C showed the smallest hydrogen adsorption peak. The large capacitive charging current indicates the activation of H_2O on Ru sites.[36] ECA values determined from the waves in the hydrogen adsorption region of the CV curves are plotted as a function of NP bimetallic composition in Figure 5B, revealing a maximum value [148 $m^2/(g$ of Pt)] for $Pt_{49}Ru_{51}/C$. This shows that the ECA depends strongly on the bimetallic composition.

In Figure 6A, the comparison of CV curves in N_2-saturated 0.1 M $HClO_4$ electrolyte with 0.5 M ethanol for different PtRu compositions shows a clear difference in the ethanol oxidation peak currents and potentials. For $Pt_{49}Ru_{51}/C$ and $Pt_{75}Ru_{25}/C$, the two ethanol oxidation peaks are observed at 0.40 and 0.65 V, characteristic of electrochemical ethanol oxidation.[20] Note that very small ethanol oxidation peaks were observed for $Pt_{31}Ru_{69}/C$. To assess the EOR activity, peak potentials are compared for different compositions in Figure 7A, and peak currents normalized to the mass of Pt are compared in Figure 7B. For both $E_{p,f}$ and $E_{p,b}$, the increase of Pt percentage resulted in higher peak potentials, which is consistent with the ability of Ru to lower the overpotential.[20]

On the other hand, $Pt_{49}Ru_{51}/C$ has higher $I_{p,f}$ and $I_{p,b}$ values than the other two compositions. The $I_{p,b}$ and $I_{p,f}$ values of $Pt_{49}Ru_{51}/C$ are 336 and 410 A/(g of Pt), respectively, which are higher than peak currents reported in the literature [$Pt_{52}Ru_{48}/C$, ~190 and ~310 A/(g of Pt)].[37] The trend $Pt_{49}Ru_{51}/C > Pt_{75}Ru_{25}/C > Pt_{31}Ru_{69}/C$, is in agreement with the ECA trend discussed earlier and previous results.[19,37,38]

$Pt_{49}Ru_{51}/C$ was found to exhibit the highest EOR activity. By comparing the composition dependences for the electrocatalytic properties in Figure 7 and the structural characteristics in Figure 4, one can see that this activity maximum appears to correlate with the maximum of the Ru−Ru bond length, the minimum of the Pt−Pt bond length, the maximum of the Pt−Ru first coordination number, and the minimum of the Pt−Pt first coordination number. This correlation provides some new insight into the composition−structure−activity relationship for the EOR in an acidic electrolyte.

After 30 potential cycles between 0 and 0.90 V (vs Ag/AgCl, saturated KCl) in N_2-saturated 0.1 M $HClO_4$ with 0.5 M ethanol, the catalytic activity of Pt_nRu_{100-n}/C (n = 31, 49, and 75) catalysts was evaluated by CV (Figure 6B). The peak potentials and peak currents for different PtRu compositions are compared in Figure 7. Remarkably, $Pt_{31}Ru_{69}/C$ and $Pt_{49}Ru_{51}/C$ showed different degrees of activity improvement after 30 cycles, with the improvement for $Pt_{49}Ru_{51}/C$ being more significant. $Pt_{75}Ru_{25}/C$ barely showed any activity change. To assess the composition change of the catalysts after the potential cycles, the composition was measured using ICP-AES. A change in the composition of $Pt_{49}Ru_{51}/C$ was found, indicating 54% Pt and 46% Ru. This finding suggests a small degree of leaching of Ru from the catalyst after 30 cycles.

The stability of the Pt_nRu_{100-n}/C catalysts was further examined by potential cycling up to 800 cycles. Peak potentials and peak currents of ethanol oxidation were measured every 50 cycles; they are plotted as functions of the number of potential cycles in Figure S1. Both the peak potentials and the peak currents increased for $Pt_{31}Ru_{69}/C$, $Pt_{49}Ru_{51}/C$, and $Pt_{75}Ru_{25}/C$. These change happened mostly in the first 100 cycles. After 150 cycles, the values seemed to reach a plateau. $Pt_{49}Ru_{51}/C$ showed the highest peak potentials and the most dramatic increases in peak current, namely, 60% and 124% for $I_{p,f}$ and $I_{p,b}$, respectively.

These findings represent the first observation of an activity increase for the EOR over PtRu catalysts by potential cycling under the experimental conditions. Based on the structural characterization, the evolution of the atomic structure and composition of PtRu NPs likely occurs during the EOR, in addition to the removal of residual surface species. These observations and preliminary results from studies of the EOR in alkaline electrolytes ruled out the effects of the removal of surface species on the activity. Rather, the structural evolution of the nanoalloys during the potential cycling is the likely reason for the observed activity change. This scenario was further examined by the in situ HE-XRD/EDX techniques, as described below.

3.3. In Situ HE-XRD/PDF/EDX of Catalysts inside MEA in an Ethanol Vapor Fuel Cell.

Having established the composition−activity correlation under ex situ conditions, the activity and stability of fresh $Pt_{49}Ru_{51}/C$ were examined in situ under EOR conditions within the MEA in a custom-built fuel cell (see Figure 8). Three percent H_2 was purged to the cathode of fuel cell, establishing a dynamic hydrogen electrode (DHE). The configuration of the XRD beam pathway was described previously.[29,39] The structure and composition evolutions were also measured by in situ HE-XRD/EDX coupled to atomic PDF analysis. Data were recorded every 1 min as the potential of the electrode with the $Pt_{49}Ru_{51}/C$ catalyst was cycled between 0 and 1.2 V at a scan rate of 100 mV/s for about 90 min, including operating time. During cycling, the cell was kept at 75 °C.

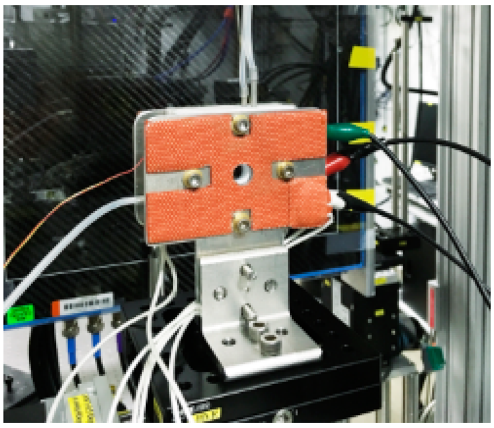

Figure 8. Setup of an ethanol vapor fuel cell for in situ HE-XRD/PDF/EDX measurements. Ethanol vapor was carried by N_2 at 50 mL/min and introduced into the anode half cell, and 3% H_2 balanced by N_2 with a flow rate of 50 mL/min was introduced into the cathode half cell, establishing a DHE for the half-cell measurements.

Our study focused on the half-cell EOR in the above fuel-cell setup for in situ EOR measurements. Note that studies of half-cell reactions in a similar fuel-cell setup have been reported for impedance measurements.[40,41] In the CV curves (see Figure S2), the EOR peak in the scan going from high potential to low potential can be observed between 0.4 and 0.8 V [vs reversible hydrogen electrode (RHE)]. There is a significant shift in the CV baseline. The peak potential and current as functions of potential cycle number are shown in Figure 9. Remarkably, both $E_{p,b}$ and $I_{p,b}$ exhibited a sharp drop in the first 60 cycles, which was not observed in our study in the electrolyte. After 60 cycles, both $E_{p,b}$ and $I_{p,b}$ gradually increased until the 200th cycle, in agreement with the results of our stability study in acidic electrolyte. The drop might reflect unique behavior for the activation of the catalyst in the ethanol vapor environment. It could take more cycles for the catalyst in the MEA to

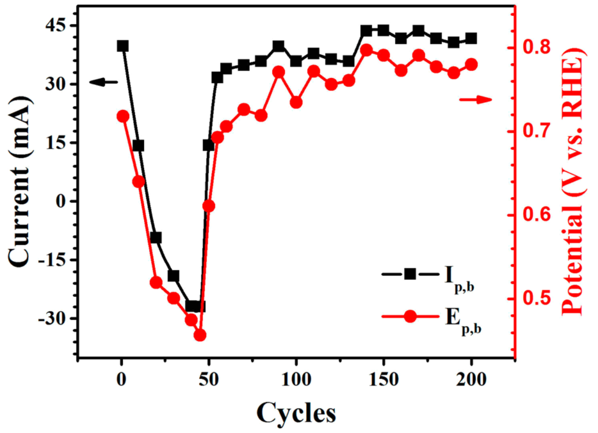

Figure 9. Plots of $E_{p,b}$ and $I_{p,b}$ as functions of potential cycle numbers for $Pt_{49}Ru_{51}/C$ in the in situ experiments (see Figure 8).

function effectively because of possibly slower mass transport through the membrane electrode assembly in the cell.

Based on an analysis of the in situ HE-XRD data (Figure S3), atomic PDFs of the $Pt_{49}Ru_{51}$ NPs were obtained to trace the atomic-level structural changes during the in situ experiments (Figure 10A). Experimental values of the atomic bond lengths and fcc stacking fault ratio were calculated and expressed as functions of the number of cycles (Figure 10B,C). Composition fluctuations experienced by the sample during the in situ EOR were evaluated by analyzing the in situ EDX spectra. The latter were calibrated against the ICP-AES data for fresh $Pt_{49}Ru_{51}/C$ and the catalyst after 200 cycles. As shown in Figure 10C, the percentage of Pt in $Pt_{49}Ru_{51}$ showed subtle changes during the in situ EOR. The Pt percentage was found to be 59% after 200 cycles. This increase in Pt percentage agrees with the results shown for the same catalyst in acidic electrolyte. The changes in Pt percentage are compared with the changes in the in situ PDFs [$G(r)$] in Figure 10B. The data in Figure 10C were extracted from the in situ PDFs shown in Figure 10B. In particular, the data points in red show the changes in the character of the packing of atomic layers in the catalysts as a function of the number of potential cycles. As can be seen, the character of packing, perfect fcc-type vs stacking faults of hcp character, changed in sync with the changes in the relative Pt percentage in the catalyst. The evolution of the average bond lengths in PtRu NPs coincides with changes in the $I_{p,b}$ values of the CV curve, indicating a clear composition−structure−catalytic activity relationship.

The data in Figure 11 were extracted from Figures 9 and 10. As shown in Figure 11A, the activity of the PtRu catalysts dropped during the first 45 cycles, likely due to repacking of the atomic layers in the catalyst, which, in turn, was triggered by the moderate leaching of Ru from the latter. During the cycles 45−60, both $E_{p,b}$ and $I_{p,b}$ increased. Concurrently, the bond lengths and thus the interactions between Pt and Ru atoms also increased. Evidently, the EOR activity of the PtRu NPs improves with the increase in the fcc character of the packing of the atomic layers in the NPs. The change in Pt percentage probably reflects a dealloying−realloying process as Ru leaches out during potential cycling.

The peak potentials ($E_{p,b}$) and peak currents ($I_{p,b}$) showed an overall trend of increase from cycle 60 to cycle 200 (Figure 11B). A "slow-mode-oscillation" behavior can be observed that is reminiscent of that of PdNi studied during the oxygen reduction reaction (ORR) under cell operating conditions.[42]

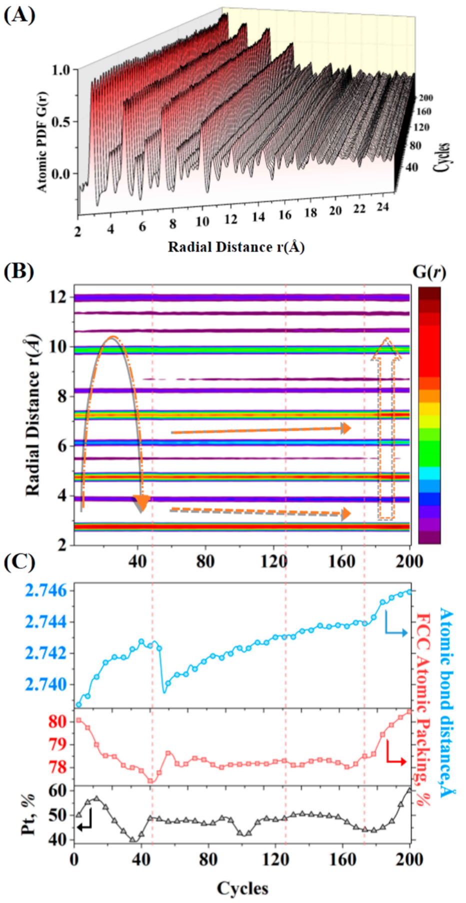

Figure 10. (A) In situ atomic PDFs of the $Pt_{49}Ru_{51}/C$ sample as a function of cycle number derived from the corresponding in situ HE-XRD patterns. (B) Color map representation of the low-r part of the in situ atomic PDFs for the sample $Pt_{49}Ru_{51}/C$ in the MEA of the ethanol vapor fuel cell. The curved arrow highlights the changes in the PDF intensity [$G(r)$] up to 45 cycles. The oblique arrows highlight the gradual changes in the position r (Å) of the PDF peaks. The outlined arrow at the right highlights the changes in PDF intensity. Dashed red lines guide the comparison between the color map of the in situ PDFs and the analysis curves with cycle number. The changes in the PDF are related to the structural changes that affect the EOR activity. (C) (Top, blue) Evolution of the average bond length during in situ EOR, which is related to the change in relative Pt percentage (bottom, black), hence changing the fcc/hcp stacking ratio (middle, red).

Other concurrent changes in the chemical composition, structural characteristics, and catalytic activity were also observed (cycles 45, 60, 120, and 180). The first 60 cycles are possibly responsible for the activation of the catalyst, which is different from the structural evolution in the subsequent cycles 60−200. For example, removal of the capping agent might expose catalysts to a higher voltage and result in a different structural change. Further discussion of the slow-mode-oscillation behavior during the realloying and subtle resizing process on the NP surface is presented in the next subsection.

4. MECHANISTIC CONSIDERATIONS

Note that there are subtle differences between the regular electrochemical conditions for the EOR in an acidic electrolyte and the conditions during the in situ study of the MEA in an ethanol vapor fuel cell, such as temperature, potential sweep range, and mass-transport environment. However, the trends in

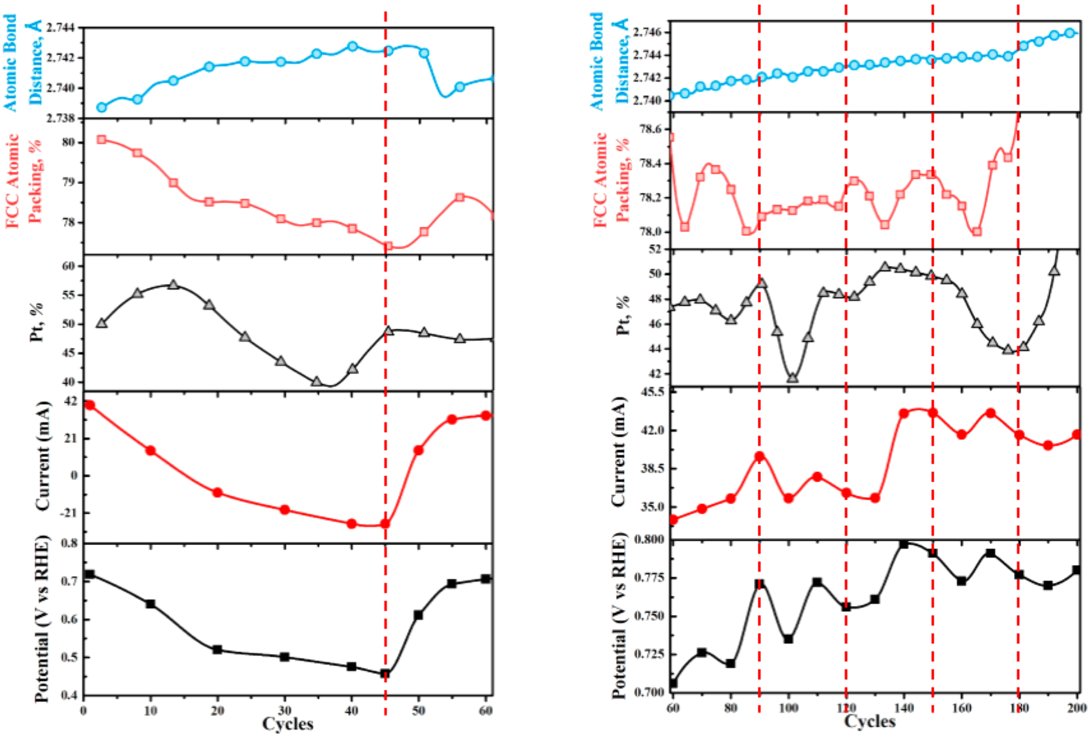

(A) (B)

Figure 11. Relationship between EOR $E_{p,b}$ and $I_{p,b}$ and the in situ evolution of the Pt percentage, fcc atomic packing percentage, and atomic bond distance for $Pt_{49}Ru_{51}/C$ in the MEA of an ethanol vapor fuel cell (see Figure 8): (A) first 60 cycles and (B) cycles 60−200. Data were extracted from Figures 9 and 10.

the voltammetric current during potential cycling are largely similar. Both cases involved Ru leaching out during potential cycling under the experimental conditions. In general, there are two major findings: (i) There is a composition−structure−activity correlation in the EOR, and (ii) there is a slow-mode-oscillation behavior for the changes in fcc atomic packing percentage and Pt percentage in the potential cycling process.

Both findings have a strong relationship to Ru leaching from PtRu/C during the EOR electrocatalytic process. Consider $Pt_{49}Ru_{51}$ as an example. This sample showed not only the highest EOR catalytic activity but also the most dramatic change during potential cycling. The potential cycling induced Ru leaching, leading to oscillatory structural evolution in terms of the fcc atomic packing percent. The alloy characteristic structure still remained during this reconstruction (realloying). The in situ HE-XRD/PDF/EDX characterization provides additional information for understanding the evolution of the structure and composition during the EOR. The dependencies on the number of cycles for fcc packing percentage and peak current show the effects on structure and activity of the Ru leaching and realloying processes. We consider two possible scenarios for Ru leaching from $Pt_{49}Ru_{51}$ under the EOR experimental conditions. One involves the realloying of Ru with Pt on the surface during cycling, and the other involves the formation of a Pt-rich shell; both are reminiscent of other nanoalloy catalysts in other electrocatalytic processes.[27,29,42]

To further substantiate the dependence of the electrocatalytic activity on composition, the $I_{p,b}$ values of the Pt_nRu_{100-n}/C (n = 31, 49, 54, and 75) catalysts in acidic electrolyte were analyzed (Figure S4). For $Pt_{49}Ru_{51}/C$ after 30 potential cycles, which resulted in $Pt_{54}Ru_{46}/C$, the highest activity was found to be reached at about 60% Pt. The trend in Figure S4 explains the activity improvement for the catalyst after 200 potential cycles from the in situ fuel cell as a result of the composition change to $Pt_{59}Ru_{41}/C$. The surface structural change due to the composition change resulting from Ru leaching during the EOR played an important role in improving the catalytic activity.

The results from the in situ HE-XRD experiments provide some important insights into the evolution of the structure and composition involving Ru leaching and during the EOR. In the MEA, Ru was leached out and remained in the vicinity of $Pt_{49}Ru_{51}/C$, instead of being diffused into the electrolyte, thus favoring realloying during in situ experiments. In Figure 12A, the catalytic activity and surface structure characteristics are compared in terms of their dependencies on the bimetallic composition.

At a Pt/Ru ratio of ∼50:50, the highest Pt−Ru first CN and the lowest Pt−Pt first CN appear to coincide with the highest catalytic activity for ethanol oxidation. It is believed that the maximization of Ru atoms in the closest neighborhood of each surface Pt atom favors the catalytic sites that provide OH(ad) for the EOR. Note that the Ru realloyed on the surface, as revealed by the in situ data, could also increase Pt−Ru first CN, leading to an increased activity.

Mechanistically, the adsorption of ethanol on the top site of Pt on the PtRu alloy surface could undergo either α-dehydrogenation or β-dehydrogenation during the EOR (see Figure 12B).[43] In a number of previous studies, PtRu catalysts were shown to exhibit no selectivity for CO_2 product formation.[20] It is thus likely that α-dehydrogenation is the predominant reaction pathway. In this case, the catalytic activity is favored by the maximization of Ru atoms around each Pt atom on the surface of the catalyst with a Pt/Ru ratio of ∼50:50

DOI: 10.1021/acs.jpcc.7b03901
J. Phys. Chem. C XXXX, XXX, XXX−XXX

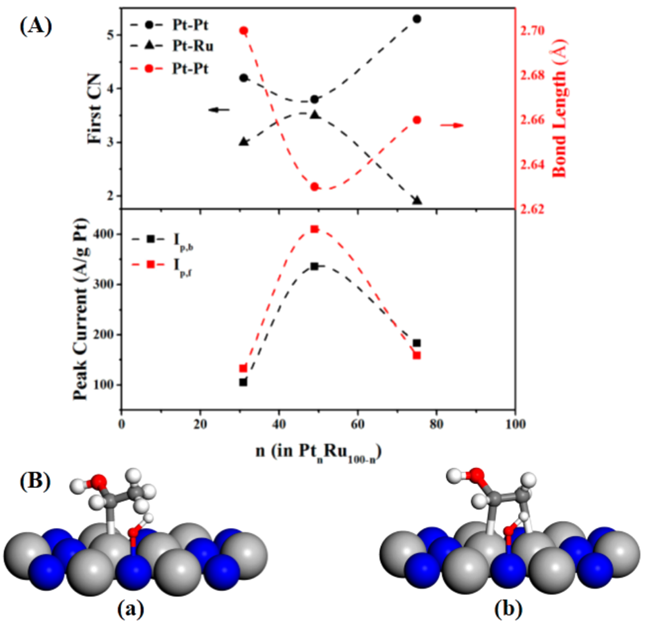

Figure 12. (A) (Top) First CN and bond length for atoms on the surface of Pt_nRu_{100-n}/C (n = 31, 49, and 75) catalysts and (bottom) $I_{p,b}$ and $I_{p,f}$ for Pt_nRu_{100-n}/C (n = 31, 49, and 75) catalysts. (B) (a) Top-site adsorption and α-dehydrogenation of ethanol. (b) Bridge-site adsorption and β-dehydrogenation of ethanol. The models are based on $Pt_{49}Ru_{51}$ with the same number of Pt and Ru atoms. Pt atoms are in gray, and Ru atoms are in blue.

where α-dehydrogenation occurs (structure a in Figure 12B). This case is consistent with the structure−composition−activity correlation shown in Figure 12A. If β-dehydrogenation occurred on the same surface site, the formation of a bridge adsorption mode (Figure 12B, structure b) would be possible. In this case, the catalytic activity would also be favored by the reduction of the Pt−Pt bond length on the catalyst with a Pt/Ru ratio of ∼50:50, leading to CO_2 product formation. This possibility would be supported by the minimization of the Pt−Pt bond length shown in Figure 12A. Details on how these different mechanisms operate in terms of catalyst synthesis and processing conditions as well as the surface coordination number and interatomic bond length for the chemisorption of alcohol[44,45] remain to be further investigated, which is part of our future work.

5. CONCLUSIONS

Taken together, the results from the electrocatalytic evaluation of the EOR, ICP-AES composition analysis, and in situ HE-XRD/PDF/EDX study of PtRu catalysts with different bimetallic compositions have provided some new insights into the correlation among the composition, atomic structure, and catalytic activity of these catalysts. The enhanced EOR activity for the catalyst with a Pt/Ru ratio of ∼50:50 correlates well with several features of the surface atomic structure, such as an increased Ru−Ru bond length, a decreased Pt−Pt bond length, an increased Pt−Ru first coordination number, and a decreased Pt−Pt first coordination number, as revealed by ex situ HE-XRD/PDF data. Importantly, the structural information can be related to the α-dehydrogenation or β-dehydrogenation of ethanol, demonstrating the potential of manipulating the interatomic coordination numbers and distances of bimetallic nanoalloy catalysts toward the control of catalytic activity and selectivity. The leaching of Ru from PtRu catalysts during potential cycling was found to be related to structural evolution based on in situ HE-XRD/PDF/EDX data. The results reveal an oscillatory characteristic in the potential cycling processes for the Pt percentage, fcc packing percentage, and EOR peak current, which is linked to Ru leaching and realloying under the EOR experimental conditions. These findings have important implications for understanding how the evolution of the structure and composition can be exploited to enhance the catalytic activity of nanoalloy catalysts in fuel-cell reactions. A study of the catalysts in direct ethanol fuel cells, similar to the study of direct methanol fuel cells,[46] is part of our future work.

■ ASSOCIATED CONTENT

Ⓢ Supporting Information

The Supporting Information is available free of charge on the ACS Publications website at DOI: 10.1021/acs.jpcc.7b03901.

> Additional data including EOR peak potentials and currents as functions of the number of potential cycles, CV curves, in situ HE-XRD pattern, and EOR peak current vs bimetallic composition (PDF)

■ AUTHOR INFORMATION

Corresponding Authors

*E-mail: cjzhong@binghamton.edu.
*E-mail: petko1vg@cmich.edu.

ORCID

Valeri Petkov: 0000-0002-6392-7589
Chuan-Jian Zhong: 0000-0003-0746-250X

Notes

The authors declare no competing financial interest.

■ ACKNOWLEDGMENTS

This work was supported by DOE-BES Grant DE-SC0006877 and by the National Science Foundation (CHE 1566283). Synchrotron X-ray diffraction experiments were carried out at beamline 11-ID-C of the Advanced Photon Source, a U.S. Department of Energy (DOE) Office of Science User Facility operated for the DOE Office of Science by Argonne National Laboratory under Contract DE-AC02-06CH11357.

■ REFERENCES

(1) Zhou, W. J.; Zhou, B.; Li, W. Z.; Zhou, Z. H.; Song, S. Q.; Sun, G. Q.; Xin, Q.; Douvartzides, S.; Goula, M.; Tsiakaras, P. Performance Comparison of Low-temperature Direct Alcohol Fuel Cells with Different Anode Catalysts. *J. Power Sources* **2004**, *126*, 16−22.

(2) Tadanaga, K.; Furukawa, Y.; Hayashi, A.; Tatsumisago, M. Direct Ethanol Fuel Cell Using Hydrotalcite Clay as a Hydroxide Ion Conductive Electrolyte. *Adv. Mater.* **2010**, *22*, 4401−4404.

(3) Beden, B.; Morin, M. C.; Hahn, F.; Lamy, C. "In Situ" Analysis by Infrared Reflectance Spectroscopy of the Adsorbed Species Resulting from the Electrosorption of Ethanol on Platinum in Acid Medium. *J. Electroanal. Chem. Interfacial Electrochem.* **1987**, *229*, 353−366.

(4) Gao, P.; Chang, S.-C.; Zhou, Z. M.; Weaver, M. J. Electrooxidation Pathways of Simple Alcohols at Platinum in Pure Nonaqueous and Concentrated Aqueous Environments as Studied by Real-time FTIR Spectroscopy. *J. Electroanal. Chem. Interfacial Electrochem.* **1989**, *272*, 161−178.

(5) Perez, J. M.; Beden, B.; Hahn, F.; Aldaz, A.; Lamy, C. "In Situ" Infrared Reflectance Spectroscopic Study of the Early Stages of Ethanol Adsorption at a Platinum Electrode in Acid Medium. *J. Electroanal. Chem. Interfacial Electrochem.* **1989**, *262*, 251−261.

(6) Iwasita, T.; Rasch, B.; Cattaneo, E.; Vielstich, W. A Sniftirs Study of Ethanol Oxidation on Platinum. *Electrochim. Acta* **1989**, *34*, 1073−1079.

(7) Iwasita, T.; Pastor, E. A Dems and FTIR Spectroscopic Investigation of Adsorbed Ethanol on Polycrystalline Platinum. *Electrochim. Acta* **1994**, *39*, 531−537.

(8) Hitmi, H.; Belgsir, E. M.; Léger, J.-M.; Lamy, C.; Lezna, R. O. A Kinetic Analysis of the Electro-oxidation of Ethanol at a Platinum Electrode in Acid Medium. *Electrochim. Acta* **1994**, *39*, 407−415.

(9) Shin, J.; Tornquist, W. J.; Korzeniewski, C.; Hoaglund, C. S. Elementary Steps in the Oxidation and Dissociative Chemisorption of Ethanol on Smooth and Stepped Surface Planes of Platinum Electrodes. *Surf. Sci.* **1996**, *364*, 122−130.

(10) Iwasita, T.; Dalbeck, R.; Pastor, E.; Xia, X. Progress in the Study of Electrocatalytic Reactions of Organic Species. *Electrochim. Acta* **1994**, *39*, 1817−1823.

(11) Xia, X. H.; Liess, H.-D.; Iwasita, T. Early Stages in the Oxidation of Ethanol at Low Index Single Crystal Platinum Electrodes. *J. Electroanal. Chem.* **1997**, *437*, 233−240.

(12) Fujiwara, N.; Friedrich, K. A.; Stimming, U. Ethanol Oxidation on PtRu Electrodes Studied by Differential Electrochemical Mass Spectrometry. *J. Electroanal. Chem.* **1999**, *472*, 120−125.

(13) Song, S.; Zhou, W.; Zhou, Z.; Jiang, L.; Sun, G.; Xin, Q.; Leontidis, V.; Kontou, S.; Tsiakaras, P. Direct Ethanol PEM Fuel Cells: The Case of Platinum Based Anodes. *Int. J. Hydrogen Energy* **2005**, *30*, 995−1001.

(14) Zhou, W.; Li, W.; Song, S.; Zhou, Z.; Jiang, L.; Sun, G.; Xin, Q.; Poulianitis, K.; Kontou, S.; Tsiakaras, P. Bi- and Tri-metallic Pt-based Anode Catalysts for Direct Ethanol Fuel Cells. *J. Power Sources* **2004**, *131*, 217−223.

(15) Gupta, S. S.; Datta, J. A Comparative Study on Ethanol Oxidation Behavior at Pt and PtRh Electrodeposits. *J. Electroanal. Chem.* **2006**, *594*, 65−72.

(16) Kowal, A.; Li, M.; Shao, M.; Sasaki, K.; Vukmirovic, M.; Zhang, J. N.; Marinkovic, N.; Liu, P.; Frenkel, I.; Adzic, R. Ternary Pt/Rh/SnO_2 Electrocatalysts for Oxidizing Ethanol to CO_2. *Nat. Mater.* **2009**, *8*, 325−330.

(17) Yin, J.; Shan, S.; Ng, M.; Yang, L. F.; Mott, D.; Fang, W.; Kang, N.; Luo, J.; Zhong, C. J. Catalytic and Electrocatalytic Oxidation of Ethanol over Palladium-Based Nanoalloy Catalysts. *Langmuir* **2013**, *29*, 9249−9258.

(18) Schmidt, V.; Ianniello, R.; Pastor, E.; Gonzalez, S. Electrochemical Reactivity of Ethanol on Porous Pt and PtRu: Oxidation/Reduction Reactions in 1 M $HClO_4$. *J. Phys. Chem.* **1996**, *100*, 17901−17908.

(19) Camara, G. A.; de Lima, R.; Iwasita, T. Catalysis of Ethanol Electrooxidation by PtRu: The Influence of Catalyst Composition. *Electrochem. Commun.* **2004**, *6*, 812−815.

(20) Wang, H.; Jusys, Z.; Behm, R. Ethanol Electro-oxidation on Carbon-supported Pt, PtRu and Pt_3Sn Catalysts: A Quantitative DEMS Study. *J. Power Sources* **2006**, *154*, 351−359.

(21) Spinace, E.; Neto, A.; Vasconcelos, T.; Linardi, M. Electro-oxidation of Ethanol Using PtRu/C Electrocatalysts Prepared by Alcohol-reduction Process. *J. Power Sources* **2004**, *137*, 17−23.

(22) Pires, F.; Corradini, P.; Paganin, V.; Antolini, E.; Perez, J. Effect of the Degree of Alloying of PtRu/C (1:1) Catalysts on Ethanol Oxidation. *Ionics* **2013**, *19*, 1037−1045.

(23) Zignani, S. C.; Baglio, V.; Sebastián, D.; Siracusano, S.; Aricò, A. S. Enhancing Ethanol Oxidation Rate at PtRu Electro-catalysts Using Metal-oxide Additives. *Electrochim. Acta* **2016**, *191*, 183−191.

(24) Sebastián, D.; Serov, A.; Matanovic, I.; Artyushkova, K.; Atanassov, P.; Aricò, A. S.; Baglio, V. Insights on the Extraordinary Tolerance to Alcohols of Fe-N-C Cathode Catalysts in Highly Performing Direct Alcohol Fuel Cells. *Nano Energy* **2017**, *34*, 195−204.

(25) Prasai, B.; Ren, Y.; Shan, S.; Zhao, Y.; Cronk, H.; Luo, J.; Zhong, C. J.; Petkov, V. Synthesis-atomic-structure-properties Relationships in Metallic Nanoparticles by Total Scattering Experiments and 3D Computer Simulations: Case of Pt−Ru Nanoalloy Catalysts. *Nanoscale* **2015**, *7*, 8122−8134.

(26) Dash, P.; Bond, T.; Fowler, C.; Hou, W.; Coombs, N.; Scott, R. Rational Design of Supported PdAu Nanoparticle Catalysts from Structured Nanoparticle Precursors. *J. Phys. Chem. C* **2009**, *113*, 12719−12730.

(27) Shen, S.; Zhao, T.; Xu, J.; Li, Y. Synthesis of PdNi Catalysts for the Oxidation of Ethanol in Alkaline Direct Ethanol Fuel Cells. *J. Power Sources* **2010**, *195*, 1001−1006.

(28) Petkov, V.; Prasai, B.; Shan, S.; Ren, Y.; Wu, J.; Cronk, H.; Luo, J.; Zhong, C. J. Structural Dynamics and Activity of Nanocatalysts Inside Fuel Cells by in Operando Atomic Pair Distribution Studies. *Nanoscale* **2016**, *8*, 10749−10767.

(29) Wu, J.; Shan, S.; Petkov, V.; Prasai, B.; Cronk, H.; Joseph, P.; Luo, J.; Zhong, C. J. Composition−Structure−Activity Relationships for Palladium-Alloyed Nanocatalysts in Oxygen Reduction Reaction: An Ex-Situ/In-Situ High Energy X-ray Diffraction Study. *ACS Catal.* **2015**, *5*, 5317−5327.

(30) Petkov, V.; Prasai, B.; Ren, Y.; Shan, S.; Luo, J.; Joseph, P.; Zhong, C. J. Solving the Nanostructure Problem: Exemplified on Metallic Alloy Nanoparticles. *Nanoscale* **2014**, *6*, 10048−10061.

(31) Alayoglu, S.; Nilekar, A.; Mavrikakis, A.; Eichhorn, B. Ru−Pt Core−Shell Nanoparticles for Preferential Oxidation of Carbon Monoxide in Hydrogen. *Nat. Mater.* **2008**, *7*, 333−338.

(32) Matin, M.; Lee, E.; Kim, H.; Yoon, W.; Kwon, Y. Rational Syntheses of Core−shell Fe@(PtRu) Nanoparticle Electrocatalysts for the Methanol Oxidation Reaction with Complete Suppression of CO-poisoning and Highly Enhanced Activity. *J. Mater. Chem. A* **2015**, *3*, 17154−17164.

(33) Xu, X.; Zhou, Y.; Lu, J.; Tian, X.; Zhu, H.; Liu, J. Single-step Synthesis of PtRu/N-doped Graphene for Methanol Electrocatalytic Oxidation. *Electrochim. Acta* **2014**, *120*, 439−451.

(34) Xiao, M.; Feng, L.; Zhu, J.; Liu, C.; Xing, W. Rapid Synthesis of a PtRu Nano-sponge with Different Surface Compositions and Performance Evaluation for Methanol Electrooxidation. *Nanoscale* **2015**, *7*, 9467−9471.

(35) Zheng, J.; Li, S.; Chen, F.; Bao, N.; Wang, A.; Chen, J.; Feng, J. Facile Synthesis of Platinum−ruthenium Nanodendrites Supported on Reduced Graphene Oxide with Enhanced Electrocatalytic Properties. *J. Power Sources* **2014**, *266*, 259−267.

(36) Li, H.; Sun, G.; Cao, L.; Jiang, L.; Xin, Q. Comparison of Different Promotion Effect of PtRu/C and PtSn/C Electrocatalysts for Ethanol Electro-oxidation. *Electrochim. Acta* **2007**, *52*, 6622−6629.

(37) Liu, Z.; Ling, X.; Su, X.; Lee, J.; Gan, L. Preparation and Characterization of Pt/C and Pt−Ru/C Electrocatalysts for Direct Ethanol Fuel Cells. *J. Power Sources* **2005**, *149*, 1−7.

(38) Camara, G. A.; de Lima, R. B.; Iwasita, T. The Influence of PtRu Atomic Composition on the Yields of Ethanol Oxidation: A Study by In Situ FTIR Spectroscopy. *J. Electroanal. Chem.* **2005**, *585*, 128−131.

(39) Redmond, E.; Setzler, B.; Juhas, P.; Billinge, S.; Fuller, T. In-Situ Monitoring of Particle Growth at PEMFC Cathode under Accelerated Cycling Conditions. *Electrochem. Solid-State Lett.* **2012**, *15*, B72−B74.

(40) Ekdharmasuit, P.; Therdthianwong, A.; Therdthianwong, S. Anode Structure Design for Generating High Stable Power Output for Direct Ethanol Fuel Cells. *Fuel* **2013**, *113*, 69−76.

(41) Ekdharmasuit, P.; Therdthianwong, A.; Therdthianwong, S. The Role of an Anode Microporous Layer in Direct Ethanol Fuel Cells at Different Ethanol Concentrations. *Int. J. Hydrogen Energy* **2014**, *39*, 1775−1782.

(42) Strasser, P.; Koh, S.; Anniyev, T.; Greeley, J.; More, K.; Yu, C.; Liu, Z.; Kaya, S.; Nordlund, D.; Ogasawara, H.; Toney, M. F.; Nilsson, A. A. Lattice-strain Control of the Activity in Dealloyed Core−Shell Fuel Cell Catalysts. *Nat. Chem.* **2010**, *2*, 454−460.

(43) Sheng, T.; Lin, W.-F.; Hardacre, C.; Hu, P. Significance of β-dehydrogenation in Ethanol Electro-oxidation on Platinum Doped with Ru, Rh, Pd, Os and Ir. *Phys. Chem. Chem. Phys.* **2014**, *16*, 13248−13254.

(44) Gasteiger, H.; Markovic, N.; Ross, P., Jr.; Cairns, E. Electro-oxidation of Small Organic Molecules on Well-characterized Pt−Ru Alloys. *Electrochim. Acta* **1994**, *39*, 1825−1832.
(45) Lamy, C.; Lima, A.; LeRhun, V.; Delime, F.; Coutanceau, C.; Leger, J.-M. Recent Advances in the Development of Direct Alcohol Fuel Cells (DAFC). *J. Power Sources* **2002**, *105*, 283−296.
(46) Arico, A. S.; Antonucci, P. L.; Modica, E.; Baglio, V.; Kim, H.; Antonucci, V. Effect of Pt-Ru Alloy Composition on High-temperature Methanol Electro-oxidation. *Electrochim. Acta* **2002**, *47*, 3723−3732.